Title

Role of Electron-Deficient Imidazoles in Ion Transport and Conductivity in Solid-State Polymer Electrolytes

Journal

Macromolecules, 55(3)

ISSN

0024-9297

Authors

Nikolaev, Andrei
Richardson, Peter M
Xie, Shuyi
et al.

Publication Date

2022-02-08

DOI

10.1021/acs.macromol.1c01979

Peer reviewed

Role of Electron-Deficient Imidazoles on Ion Transport and Conductivity in Solid-State Polymer Electrolytes

Andrei Nikolaev, Peter M. Richardson, Shuyi Xie, Luana Llanes, Seamus D. Jones, Oscar Nordness, Hengbin Wang, Guillermo Bazan, Rachel A. Segalman*, Raphaële J. Clément*, and Javier Read de Alaniz*

ABSTRACT: Solid-state polymer electrolytes offer a safer alternative to traditional lithium-ion batteries based on organic electrolytes. The focus is here on imidazole functionalized polymer electrolytes, where the imidazole ligand promotes salt dissolution, while its functionalization allows to tune the dynamic interactions between the cations in solution and the imidazole ligand tethered to the polymer backbone. Although careful choice of polymer backbone and imidazole linker functionality have resulted in polymer electrolytes with increased total ionic conductivities and a boost in the Li^+ ion contribution, improvements in performance through modifications of the imidazole heterocycle remain underexplored. In this work, we systematically investigate poly(methylsiloxane) (PMS) polymers functionalized with a series of halogen-substituted imidazoles and show that Li^+ ion conduction can be tuned by electron-deficient heterocycle ligand. When the number of halogen substituents increases, the Li^+ ion mobility also increases as measured by pulsed-field-gradient NMR and NMR relaxometry. Although beneficial for Li^+ transport, electron-deficient imidazole ligands result in clustering, as indicated by wide-angle X-ray scattering, and poor salt dissolution, which in turn impedes the overall ionic transport. This work highlights the importance of synthetic design and the necessity for high salt solvation and weak cation-polymer binding to obtain high Li^+ transport numbers.

INTRODUCTION

The continued demand to improve the performance and the energy density of lithium(Li)-ion batteries for consumer electronics, energy storage, and electric vehicles have spurred materials innovations and research in this fast-growing field.[1–3] Despite gradual increases in the charge storage capacity of electrode materials and the overall energy density of Li-ion cells, devices based on traditional small-molecule liquid electrolytes are amenable to catching fire or exploding, as well as leakage hazards owing to the flammability and volatility of organic liquids (e.g., carbonate-based).[4,5] Solid-state electrolytes offer a safer alternative to liquid electrolytes due to their mechanical robustness and nonflammability. Specifically, inorganic- and polymer-based electrolytes have received significant attention for high energy density Li-ion batteries.[6,7] However, the processing of inorganic materials is challenging due to their hardness and brittleness, limiting their applicability. Polymeric solid-state electrolytes exhibit highly tunable chemistries and properties and provide an avenue for circumventing processability issues (e.g. brittleness). However, compared to state-of-the-art ion conductors, polymer electrolytes suffer from modest ionic diffusion properties. Ion conduction in polymers hinges on the presence of ligand groups that enable salt dissolution (i.e., solvating groups), and on dynamic interactions between cations in solid state and the ligands tethered to a polymer backbone to facilitate ion transport. One challenge is that anion transport is typically more facile than cation transport, but only the cations, such as Li^+ ions, contribute to the overall ionic current and battery performance.[8] Moreover, lithium-ligand interactions must be strong enough to dissociate the Li-containing salt but sufficiently weak to enable fast Li+ ion transport. To realize this delicate balance, the rational design of new polymeric solid-state electrolytes that exhibit highly tunable lithium-ligand interactions is needed.

We have previously demonstrated the presence of dynamic metal-ligand interactions in imidazole-containing polymers doped with lithium and other metal ion salts.[9] Recently, we have also demonstrated that removal of the hydrogen-bonding and Li^+ coordinating amide functionality in the polymer scaffold enables a 100-fold increase in the room-temperature total ionic conductivity, and a doubling of the Li^+ transport number.[10] These results suggest that there is significant room for improvement, and careful choice of polymer building blocks can results in dramatic performance enhancements.

Herein, we report on our work seeking to improve polymer electrolyte performance by modifying the electronic and steric properties of the imidazole heterocycle ligand. Using a modular synthetic approach, we introduce a series of poly(methylsiloxane) (PMS) homopolymers bearing a range of electron-deficient imidazole ligands. Using pulsed-field gradient (PFG) nuclear magnetic resonance (NMR) spectroscopy and NMR relaxometry, we show how Li-ligand coordination, and Li diffusion and transport properties depend on the number and type of electron deficient moieties substituted onto the imidazole ring. We uncover that, although the total ionic conductivity decreases relative to the parent imidazole-based material, the Li ion-mobility increases as the imidazole becomes more electron deficient and sterically bulky. These results demonstrate the important role of nitrogen heterocycles in tuning Li-ligand coordination in solid-state polymer electrolytes and provide a guide for improving Li-ion transport in these systems.

EXPERIMENTAL

PVMS synthesis.

Poly(vinyl methyl siloxane) (PVMS) was synthesized by anionic polymerization using standard Schlenk line techniques. A custom built, heavy walled reaction flask equipped with a Schlenk adaptor and a septum-sealed antechamber for needle transfers was charged with a pyrex-coated stir bar and was flame dried. 200 mL of uninhibited and dry THF was taken from a solvent still and added to this reactor. The THF was cooled to -77 °C using a dry ice/IPA bath. After confirming the flask had cooled with a thermometer, the flask was titrated with 1.3 M sec-BuLi solution in cyclohexane until a yellow color persisted, consistent with formation of the living THF anion (< 0.15mL of sec-BuLi). The flask was put under intense stirring and the reactor was gently shaken to coat all the interior surface of the flask, neutralizing any species that could quench this anion and the yellow color remained throughout this process. After 5 minutes of stirring, the cold bath was removed, and the flask was warmed using a hot water bath to ~45 °C. As the flask was warmed, the color returned to clear as the THF anion died. This flask was subsequently transferred into a nitrogen containing glovebox for the addition of monomer. The monomer (12.2 mL, 11.82 g), 1,3,5-trivinyl-1,3,5-trimethyl-cyclotrisiloxane (Gelest), was opened in a nitrogen-containing glovebox and added to the flask via a sytringe transfer. No additional purification of the monomer was performed. After monomer addition, the flask was returned to the Schlenk line and 420 µL of sec-butyl lithium was added to the reactor at 0 °C as initiator, resulting in no visible color change. The reaction was allowed to proceed for 3 hours at 0 °C before termination with degassed methanol. The solution was concentrated and precipitated in methanol three times, redissolving with THF after each precipitation step. Size exclusion chromatography (SEC) was performed on a Waters Alliance HPLC instrument using a refractive index detector and Agilent PLgel 5 µm MiniMIX-D column at 35 °C with THF as the eluent. The PVMS molecular weight M_n = 101 kg/mol and dispersity $Đ$ = 1.82 were estimated from SEC using Polystyrene standards (Agilent Technologies) (Figure S1).

Sample preparation.

Polymers were dissolved in dichloromethane (DCM) and mixed with desired amounts of stock solution of LiTFSI salt (1 wt%) in anhydrous tetrahydrofuran (BHT stabilized) to reach the desired r values. The solution was then drop-cast onto Teflon boats and dried under vacuum (~10^{-2} Torr) at room temperature for one day followed by at 50 °C for another day. The samples were then transferred into a high vacuum oven equipped with a turbopump (~10^{-8} Torr) and further dried at 50 °C for one day to ensure complete removal of solvent. All samples were kept in a nitrogen glovebox for storage and further characterizations.

Thermal characterization.

Samples (~5 mg) were loaded into Tzero Aluminum Hermetic DSC pans (TA instrument) and tested on DSC2500 (TA instrument). The glass transition temperature (T_g) of each sample was measured based on the third heating cycle between –120 to 120 °C at 20 °C/min at the midpoint of the step transition. All DSC traces for salt-free and salt-doped polymers can be found in Figure S16, and the T_g data are summarized in Table S2.

Ionic Conductivity Characterization.

Impedance measurements were performed on a Biologic VSP-300 using two ITO glass electrodes with Kapton tape as an ~ 150 µm spacer. A hole of precise diameter (4.76 mm) was punched in the tape to control the electroactive area of the sample. A second electrode was placed on top and then consolidated with a press (100 °C, 5 min). The film thicknesses were measured using a digital micrometer (+/- 1 μm precision) on the assembly with and without the polymer. Impedance measurements were performed from 1 MHz down to 0.1 Hz with an amplitude of 100 mV and the complex impedance ($Z^* = Z' - i\omega Z''$) was converted to complex conductivity according to:

$$\sigma'(\omega) = \frac{Z'(\omega)}{k[Z'(\omega)^2 + Z''(\omega)^2]}$$

The frequency independent plateau (also the maximum of tan δ) of conductivity was taken as the "DC conductivity". The conductivity as a function of 1000/T is shown in Figure S17.

Wide-angle X-ray scattering (WAXS).

Polymer samples were loaded into aluminum washers with 1 mm thickness in a nitrogen glovebox and covered with Kapton tape to prevent moisture uptake during measurement. X-ray scattering measurements were performed at the National Synchrotron Light Source II (NSLS-II, beamline 11-BM, Brookhaven National Laboratory), with an X-ray energy of 13.5 keV. The sample to detector distance was calibrated using a silver behenate standard, and 2D raw WAXS images was reduced into 1D intensity versus q curves.

Density measurement and calculation.

The density of PMS-10-Im was measured gravimetrically. The polymer was loaded into an NMR tube, followed by degassing at 50 °C under vacuum for two days. After the material settled down at the bottom of the tube, it was slowly cooled to room temperature, and the mass and volume were carefully measured. The density was calculated as 1.13 g/cm^3.

The density for each halogen-substituted polymer was then calculated using the Group Contribution Method (GCVOL) using the parameters provided by Ihmels and Gmehling,[11] and Krevelen and Hoftyzer.[12] For salt-doped polymers, the density was calculated assuming an additive volume of the polymer and salt. A summary can be found in Table S3.

PFG-NMR Measurements

Prior to measurement, NMR samples were packed under Argon and placed into vacuum sealed NMR tubes to prevent water contamination. PFG-NMR measurements were performed using a 300 MHz (7.05 T) SWB Bruker NMR spectrometer equipped with a Diff50 probe. The diffusion values for both ^{19}F and ^{7}Li nuclei were measured using a variable magnetic field gradient strength sequence with an incorporated stimulated echo to protect the signal from T_2 relaxation. Careful consideration was given to the selection of the gradient pulse duration (δ) and diffusion time (Δ) to recover the best signal for each experiment. Sample temperature was controlled by an 800 $L\,hr^{-1}$ N_2 gas flow which provided an inert atmosphere with fast temperature equilibration. The probe temperature was calibrated using pure ethylene glycol.

RESULTS AND DISCUSSION

We have recently demonstrated that the PMS homopolymer bearing imidazole ligands operates as a superior Li-ion conducting polymer electrolyte (with a Li^+ transport number (t+) = 0.43 versus a Li^+ t+ in the range of 0.1-0.3 for PEO).[10] Therefore, PMS is chosen as the polymer backbone for this study, because its highly nonpolar nature mitigates competitive solvation of the Li^+ ions and helps ensure that Li-ligand interactions can be isolated and controlled. To systematically evaluate the effect of imidazole heterocycle functionalization, we have selected a series of halogen-containing (Cl, Br, and CF_3) imidazole derivatives that are electron-withdrawing

due to induction by the halogen substituents. Although metal catalysis and medicinal chemistry have long exploited the ability to tune metal-ligand interactions for synthesis,[13–16] the use of nitrogen heterocycles in Li-ion polymer electrolytes has seldom been explored.[17,18] To construct the PMS homopolymers bearing imidazole ligands functionalized with 4,5-dichloro, 2-bromo-4,5-dichloro, 2,4,5-tribromo and 4,5-bis(trifluoromethyl) substituents, we have adapted the modular synthetic approach developed in our recent work[21] (Figure 1). First, the thiol-alkyl-heterocycle sidechains were synthesized via a nucleophilic substitution reaction between 1-bromo-7-chloroheptane (**1**) and the conjugate base of the halogenated imidazole (**2**) to access the 1-(7-chloroheptyl)-imidazole derivative (**3**), followed by a substitution reaction between 3 and sodium hydrogen sulfide (NaSH) to access the 7-(1-imidazole-derivative-1-yl)heptane-1-thiol (**4**). In a final step, a post-polymerization functionalization of poly(vinylmethylsiloxane) (PVMS) (each repeat unit has a vinyl group) (**5**) via a light-induced thiol-ene reaction between **4** and PVMS yielded the corresponding PMS polymers bearing imidazole derivatives (**6**). For clarity, the polymers are named according to the polymer backbone (PMS), number of atoms between the polymer backbone and the imidazole heterocycle (**10**) and then the number and type of halogen substituents on the imidazole (Im) (e.g., PMS-10-ImCl$_2$, **8**).

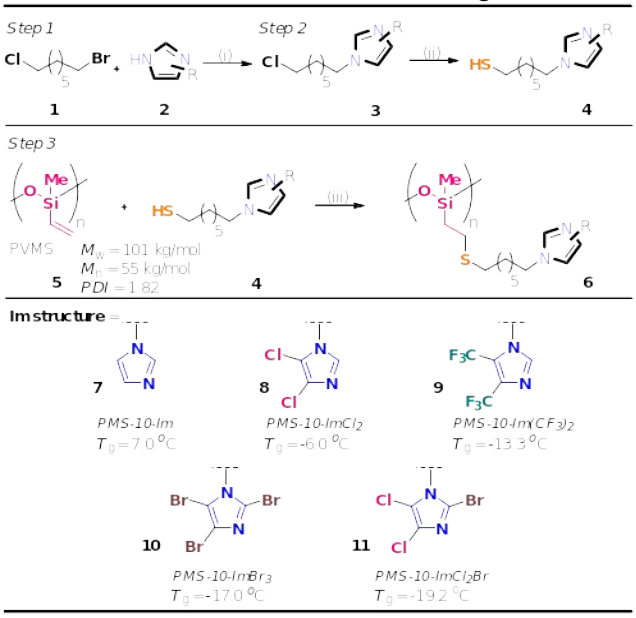

Figure 1. A modular three-step synthesis of the PMS graft polymer containing halogen-substituted imidazole ligands. (i) Base (SI), THF, rt to 65 ºC, 24 h; (ii) NaSH (1.4 equiv), MeOH, 65 ºC, 20 h; (iii) dichloromethane (DCM), DMPA (10 mol%), 365 nm, rt, 5 h.

We used the Swain-Lupton electronic-[19] and the upsilon steric parameters[20] to quantify and compare the relative electronic (field/inductive and resonance) and steric properties of H, Cl, Br, and trifluoromethyl (CF_3) substituents (Table S1). The electronic properties of substituents either arise from a field effect (electron-withdrawing through space and through intervening σ bonds) or from a resonance effect (pi electron-donating or withdrawing). Herein, the F-parameter corresponds to field and inductive effects, and the R-parameter is associated with resonance effects.[21,22] Generally, a substituent with a positive F- or R-value is electron-withdrawing, while negative values imply electron donation. For example, due to their higher electronegativity relative to hydrogen, chlorine, and bromine exhibit high inductive/field withdrawing contributions, with F = 0.42 and 0.45, respectively. In addition to the inductive-withdrawing effect, bromine and chlorine also exhibit resonance donating (pi donation) contributions of R = -0.19 and R = -0.22, respectively. These parameters indicate that bromine is slightly more inductively/field withdrawing and resonance donating than chlorine. On the other hand, the CF_3 group behaves as a purely electron-withdrawing substituent via both induction and resonance, as indicated by its positive F = 0.38 and R = 0.16 values. The inductive effects of the chlorine (F = 0.42), bromine (F = 0.45) and CF_3 (F = 0.38) substituents render the imidazole moiety more electron-deficient,

which weakens the N-Li coordinative interaction and is expected to facilitate Li^+ ion diffusion within the polymer matrix. In addition to electronic effects, steric of the chlorine (υ = 0.55), bromine (υ = 0.65), and CF_3 (υ = 0.90) substituents are also expected to facilitate the Li^+ ion diffusion by hindering the N-Li interaction relative to unsubstituted imidazole (hydrogen, υ = 0).

The series of five PMS polymers bearing a range of electron-deficient imidazole ligands were mixed with lithium bis(trifluoromethanesulfonyl)imide (LiTFSI) salt (concentration r = [Li+]/[Im] = 0.3) and electrochemical impedance spectroscopy (EIS) measurements were carried out to determine their total ionic conductivities (Figure 2). To decouple the influence of polymer segmental motion on the ionic conductivity, all data have been normalized by T_g. The EIS data reveal that all of the halogen-substituted imidazoles exhibit lower ionic conductivity as compared to the halogen-free imidazole (PMS-10-Im), despite the latter being more electron-rich. Specifically, replacing hydrogens (F = 0.03 and R = 0.00) with CF_3 (F = 0.38 and R = 0.16) substituents at positions 4 and 5 on the imidazole results in an order of magnitude decrease in conductivity (Figure 2). The ionic conductivity of the 4,5-dichloroimidazole-containing polymer (PMS-10-$ImCl_2$) lies in-between that of PMS-10-Im and PMS-10-$Im(CF_3)_2$. A further decrease in conductivity is observed for the perhalogenated imidazole analogs: PMS-10-$ImBr_3$ and PMS-10-$ImCl_2Br$. Interestingly, replacing hydrogen at the 2-position of PMS-10-$ImCl_2$ (upsilon steric parameter (υ), υ = 0) for bromine PMS-10-$ImCl_2Br$ (υ = 0.65) substantially lowers the total ionic conductivity, which we tentatively attribute to the change in sterics.

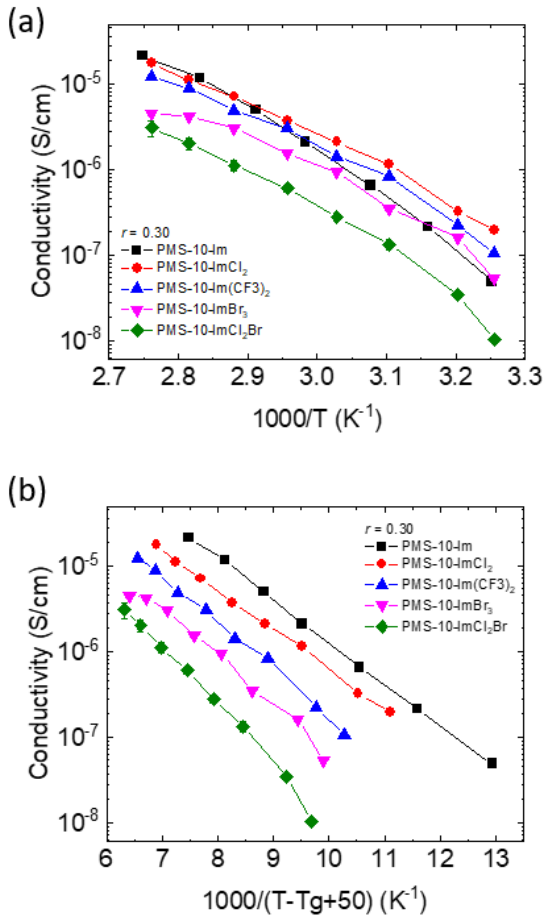

Figure 2. (a) 1000/T versus conductivity and (b) T_g-normalized ionic conductivity profiles for LiTFSI-doped PMS-10-Im, PMS-10-$ImCl_2$, PMS-10-$Im(CF_3)_2$, PMS-10-$ImBr_3$, and PMS-10-$ImCl_2Br$ polymers at a salt concentration r = 0.3, computed using the Vogel-Fulcher-Tamman (VFT) equation assuming the Vogel temperature $T_0 = T_g$ -50 °C.

Surprised by the decrease in the total ionic conductivity observed upon introduction of electron deficient imidazole ligands, we turned to wide-angle X-ray scattering (WAXS) to investigate the formation of ion pairs. Salt aggregation and ion-ion interactions are known to be detrimental to ionic conductivity.[23] We speculate that the less coordinating ligands reduce the ability to efficiently dissociate the salt ions, thus impeding ionic transport. As shown in Figure 3, at r = 0.3, multiple correlation peaks are present in all five polymers. The broad peak at 1.3-1.5 Å-1 is attributed to the 'van der Waals' or amorphous halo, which is a universal feature of polymers arising from the disordered nature of spatial segmental correlations. Note that the amorphous halo positions for the two perhalogenated imidazole analogs (PMS-10-ImBr_3 and PMS-10-ImCl_2Br) are found at larger q values than for other polymers (q ≈ 1.5 compared to 1.3 A−1), indicating that Li-ion environments in these two polymers are different from those present in the other polymer systems considered here. Another correlation peak appears for all of the four polymers with halogen-substituted ligands around 0.2-0.25 Å-1 (3.1 to 2.5 nm), as indicated by the filled upside-down triangles in Figure 3. A previous report on salt-doped imidazole-containing polymers has suggested that this peak corresponds to correlations in high salt density domains (i.e., salt aggregates),[24] indicating that ion pairing and aggregation cannot be neglected in polymers with electron-deficient ligands. Although the fraction of free ions cannot be quantified based on WAXS patterns, we conjecture that the existence of ion pairs and aggregates leads to a lower conductivity as the number of free ions is reduced. Hence, ion aggregation explains the decrease in total ionic conductivity as the ligand electron deficiency is increased. Note that another sharp peak at 0.4 Å-1 (open upside-down triangle) arises from the Kapton film, and no other sharp Bragg peak is observed in any of the polymers, indicating that LiTFSI remains amorphous in the polymer matrix.

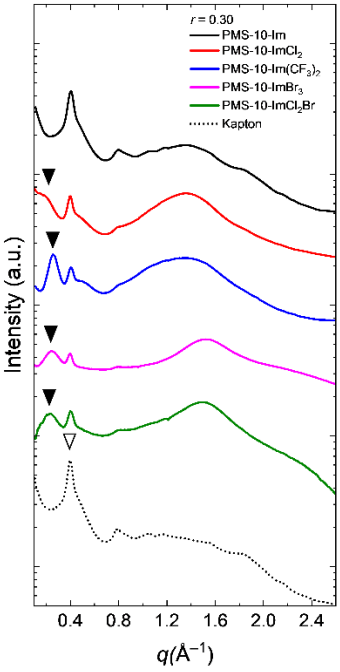

Figure 3. Wide-angle X-ray scattering profiles for polymers at 30 °C and r = 0.3.

To further study the interactions between the Li and TFSI ions, we used Raman spectroscopy to measure the vibrational spectra of CF_3 on the PMS-10-Im$(CF_3)_2$ backbone. Measurements were carried out with and without the addition of salt. As shown in Figure 4, for the salt-free polymer, the peak at 757 cm^{-1} can be assigned to symmetric vibration of CF_3 on the polymer side chain, and with the addition of salt, this peak position remains the same, indicating the salt-ligand interaction is relatively weak. At r = 0.03, a weak shoulder at 740 cm^{-1} is observed. However, increasing the salt to ligand concentration (r = 0.3) results in the development of a strong and

broad peak at 745 cm^{-1}. This peak is consistent with the vibration of the TFSI anion. Previous work has demonstrated that in LiTFSI-doped PEO or PS-b-PEO copolymer, the free TFSI ions show a Raman shift of 740 cm^{-1}, while the peak for ion pairs is around 744 cm^{-1}.[25] This result supports that ion pairing is more prevalent at a higher salt concentration and plays a major role at r = 0.3. Unfortunately, due to the resolution limit of our Raman measurements, the actual fraction of TFSI free ion is not accessible.

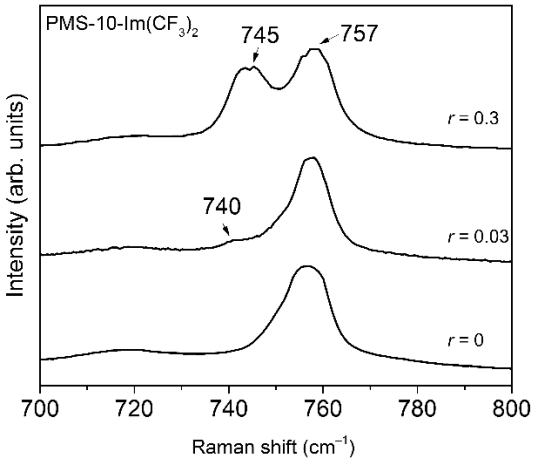

Figure 4. Raman spectra for PMS-10-Im$(CF_3)_2$ at r = 0, 0.03, and 0.3 at room temperature.

To gain insight into the influence of steric and electronic factors of electron-deficient imidazole ligands on the Li^+ and $TFSI^-$ ion mobilities, pulsed-field-gradient NMR (PFG-NMR) was employed. This technique allows the self-diffusion coefficients of these two ions to be measured separately by monitoring the diffusion of ^7Li and ^{19}F nuclei, respectively. Figure 5a shows the self-diffusion coefficients for both ions within each of the polymers measured at 84.4 °C. Given that only the Li^+ ions contribute to the overall ionic current, we focus our discussion on the properties that lead to high lithium mobility. Overall, the self-diffusion of Li^+ ions reveals that the steric and strong inductive effect of the halogen substituents enhance Li mobility (weak N-Li coordinative interaction) (Table 1). For example, replacing chlorine-substituents (Entry 2), for bulkier and more electron withdrawing trifluoromethyl-substituents (Entry 3) increased Li^+ ion diffusion from $1.65x10^{-13}$ to $2.51x10^{-13} m^2/s$, which further increases for more sterically encumbered and electron-deficient trisubstituted imidazole ligands (Entries 4 and 5). The self-diffusion values of Li^+ ions within the five polymers measured at 84.4 °C show the following trend: PMS-10-ImCl_2Br ≈ PMS-10-ImBr_3 > PMS-10-Im >PMS-10-Im$(CF_3)_2$ > PMS-10-ImCl_2. However, the weakened N-Li interaction also leads to a decrease in the total ionic conductivity (Table 1). These results are consistent with incomplete dissociation of the LiTFSI salt (ion-pairing) (Figure 3). Moreover, two distinct Li-containing diffusing species are required to fit the PFG-NMR results obtained for the PMS-10-ImBr_3 polymer system (see Figure S20), which suggests the presence of two different Li-ion environments tentatively attributed to free Li^+ ions and Li^+ ions in pairs. Importantly, plotting excess conductivity as a function of upsilon steric parameters (υ) (Figure 5b) shows a positive correlation suggesting that increase in steric environment of imidazole ring in part contributes to neutral ion-pair formation.

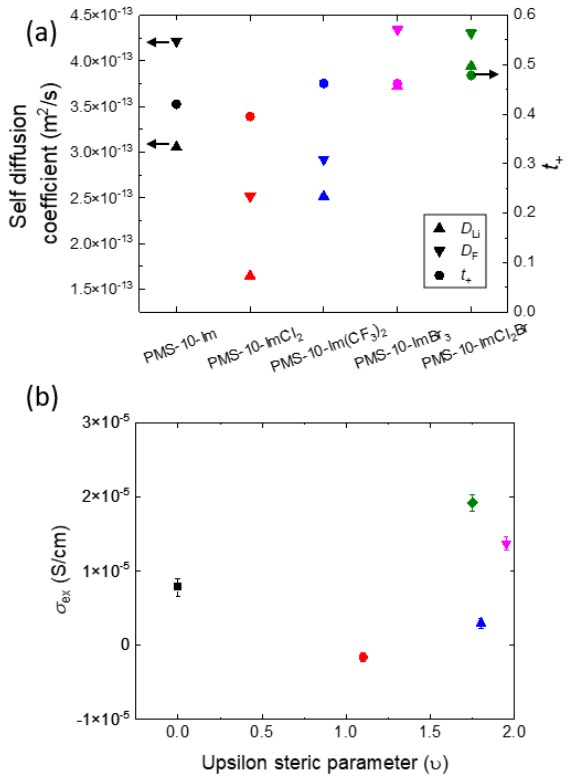

Figure 5. (a) Self-diffusion coefficients for Li-containing species, D_{Li} (triangles), F-containing species, D_F (upside down triangles) and corresponding Li^+ transport numbers, t_+ (circles) for the five polymers investigated, measured by PFG-NMR at 84.4 °C. (b) Excess conductivity ($\sigma_{ex} = \sigma_{NE} - \sigma_{EIS}$) for LiTFSI-doped PMS-10-Im, PMS-10-$ImCl_2$, PMS-10-$Im(CF_3)_2$, PMS-10-$ImBr_3$, and PMS-10-$ImCl_2Br$ polymers at a salt concentration r = 0.3 as a function of the sum of upsilon steric parameters (υ).

Next, we computed the fraction of electric current derived from the motion of the "free" Li+ ions. For this, we calculated the Li+ transport numbers ($t_{+¿¿}$) based on the PFG-NMR self-diffusion constants for the cation ($D_{+¿¿}$) and anion ($D_{-¿¿}$) measured at 84.4°C using equation 1.

$$t_{+¿=\frac{D_{+¿}}{D_{+¿+D_{-¿¿}}}¿¿} \qquad (1)$$

Table 1 summarizes the Li^+ transport numbers for all of the polymers of interest. The PMS-10-$ImCl_2Br$ polymer exhibits the highest Li^+ $t_{+¿¿}$ of 0.48. The $t_{+¿¿}$values for PMS-10-$ImBr_3$ and PMS-10-$Im(CF_3)_2$ polymers are only slightly lower at 0.46 and the PMS-10-$ImCl_2$ polymer exhibits the lowest Li-ion transport in the series. For comparison, the PMS-10-Im indicated Li^+ of 0.43. As mentioned earlier, the trends in the ionic conductivity displayed in Figure 2 and the self-diffusion coefficients in Figure 5a differ. Namely, the polymer with the fastest diffusing Li^+ ions does not correspond to the polymer electrolyte with the highest ionic conductivity. It is worth noting that, while the ionic conductivity is a measure of the movement of charged species (dissociated ions), the self-diffusion values measured by PFG-NMR account for all of the molecules that contain the nucleus of interest indiscriminate of whether these nuclei comprise dissociated ions or ion-paired ions. To quantify this effect, we calculated the Haven ratios for the six polymers in this study. The Haven ratio (H_R) is an experimental metric used to describe the extent of ion dissociation within an electrolyte system. Typically, H_R values lie between zero and one (unity), where a value of unity represents an ideal correlation between the ionic conductivity and self-diffusion measurements, i.e., as in the case of completely dissociated ions. On the other hand, a ratio less

than unity implies that some of the ions do not contribute to the conduction process, due to ion pairing.[26,27] First, the self-diffusion constants can be used to calculate the conductivity *via* the Nernst-Einstein Equation (σ_{NE}) as shown in equation 2.

$$\sigma_{NE} = N_A e^2 C ¿¿ \quad (2),$$

where N_A is Avogadro's Number, e is the charge of an electron, C is the concentration of LiTFSI in the polymer (Mol/cm^3), k_B is Boltzmann's constant and T is the sample temperature. The density of the polymers was estimated using the GCVOL (group contribution volume) method and used to calculate the salt concentration of each polymer (see ESI for calculations). The Haven ratio (H_R) is then calculated by dividing the EIS measured (σ_{EIS}) and Nernst-Einstein σ_{NE} calculated conductivities, as shown in equation 3.

$$H_R = \frac{\sigma_{EIS}}{\sigma_{NE}} \quad (3)$$

Substituent	*F*	*R*	*v*	Polymer	Li+ Diffusion (x10^{-13} m^2/s)	*t*+	□EIS (x10^{-5} S/cm)	□NE (x10^{-5} S/cm)	□□
H	0.03	0	0	PMS-10-Im	3.1	0.42	1.5	2.3	0.66
Cl	0.42	-0.19	0.55	PMS-10-ImCl$_2$	1.7	0.40	1.3	1.2	1.1
CF$_3$	0.38	0.16	0.9	PMS-10-Im(CF$_3$)$_2$	2.5	0.46	1.0	1.3	0.77
Br	0.45	-0.22	0.65	PMS-10-ImBr$_3$	3.7	0.46	0.52	2.0	0.26
Cl, Br	0.42, 0.45	-0.19, -0.22	0.55, 0.65	PMS-10-ImCl$_2$Br	3.9	0.48	0.24	2.2	0.11

Table 1. Swain-Lupton electronic parameters (*F*) and (*R*), upsilon steric parameter (υ), Li$^+$ self-diffusion constants, Li$^+$ transport numbers (t^+), total measured conductivity and Haven ratios (H_R¿ arising from Li$^+$ and TFSI$^-$ measured at 84.4 °C for the five polymers with Li/monomer = 0.3.

Table S4 summarizes the values of the self-diffusion coefficients, transport numbers, measured and calculated conductivities and the Haven Ratios for all six polymer samples at different temperatures. Of note, measurement of ion self-diffusion at temperatures below ≈ 67 °C were not possible due to the short NMR signal relaxation times of ^{7}Li and ^{19}F nuclei. The calculated Haven Ratios follow the same trend as that of the total ionic conductivity for the halogenated imidazole series: PMS-10-ImCl$_2$ > PMS-10-Im(CF$_3$)$_2$ > PMS-10-ImBr$_3$ > PMS-10-ImCl$_2$Br. These results, together with the WAXS data (Figure 3), suggest that ion pairing plays a significant role in these polymer electrolytes. Moreover, the reduced conductivity relative to PMS-10-Im suggests that there is likely an optimum Li-N interaction that dictates the level of ion dissociation in the sample.

CONCLUSION

In conclusion, we have examined a series of PMS polymers bearing electron-deficient imidazole ligands to investigate the role of ligand on metal-ligand coordination on polymer electrolyte performance. We find that an increase in halogen substituents decreases the coordinating ability of the imidazole ligand increases Li$^+$ ion diffusion from 0.43 (PMS-10-Im) to 0.48 (PMS-10-ImCl$_2$Br). However, the electron-deficient imidazole heterocycles also result in a decrease in the total ionic conductivity due to ion pairing of LiTFSI as confirmed by WAXS, Raman spectroscopy and PFG-NMR. These results highlight an important tradeoff between solvating ability and ion diffusivities when the strength of the ion-polymer interaction is tuned.

ASSOCIATED CONTENT

AUTHOR INFORMATION

Corresponding Authors

Javier Read de Alaniz − *Department of Chemistry and Biochemistry, University of California at Santa Barbara, Santa Barbara, California 93106, United States;* orcid.org/0000-0003-2770-9477; *Email:* javier@chem.ucsb.edu

Rachel A. Segalman − *Materials Department, University of California, Santa Barbara, California 93106, United States; Materials Research Laboratory, Mitsubishi Chemical Center for Advanced Materials, and Department of Chemical Engineering, University of California, Santa Barbara, California 93106, United States*; orcid.org/0000-0002- 4292-5103; Email: segalman@ucsb.edu

Raphaële J. Clément − *Materials Department, University of California, Santa Barbara, California 93106, United States; Materials Research Laboratory and Mitsubishi Chemical Center for Advanced Materials, University of California, Santa Barbara, California 93106, United States;* orcid.org/0000-0002-3611-1162; Email: rclement@ucsb.edu

Authors

Andrei Nikolaev − *Mitsubishi Chemical Center for Advanced Materials and Department of Chemistry and Biochemistry, University of California, Santa Barbara, California 93106, United States*

Peter M. Richardson − *Materials Research Laboratory and Mitsubishi Chemical Center for Advanced Materials, University of California, Santa Barbara, California 93106, United States*; orcid.org/0000-0002-6631-2459

Shuyi Xie − *Materials Research Laboratory and Mitsubishi Chemical Center for Advanced Materials, University of California, Santa Barbara, California 93106, United States;* orcid.org/0000-0001-7966-1239

Luana Llanes – *Mitsubishi Chemical Center for Advanced Materials and Department of Chemistry and Biochemistry, Center for Polymers and Organic Solids, University of California, Santa Barbara, California 93106, United States*

Seamus D. Jones − *Department of Chemical Engineering and Materials Research Laboratory, University of California−Santa Barbara, Santa Barbara, California 93106, United States*

Oscar Nordness - *Materials Research Laboratory and Mitsubishi Chemical Center for Advanced Materials, University of California, Santa Barbara, California 93106, United States*

Hengbin Wang − *Mitsubishi Chemical Center for Advanced Materials, University of California, Santa Barbara, California 93106, United States*

Notes

ACKNOWLEDGMENT

This work was supported by the MRSEC Program of the National Science Foundation under Award No. DMR 1720256 (IRG-2). The research reported here made use of shared facilities of the UC Santa Barbara MRSEC (NSF DMR 1720256), a member of the Materials Research Facilities Network (www.mrfn.org/). Any opinions, findings, and conclusions or recommendations expressed in this material are those of the authors and do not necessarily reflect the views of the National Science Foundation.

REFERENCES

(1) Nitta, N.; Wu, F.; Lee, J. T.; Yushin, G. Li-Ion Battery Materials: Present and Future. *Materials Today*. Elsevier B.V. June 1, 2015, pp 252–264.

(2) Hayner, C. M.; Zhao, X.; Kung, H. H. Materials for Rechargeable Lithium-Ion Batteries. *Annu. Rev. Chem. Biomol. Eng.* **2012**, *3* (1), 445–471.

(3) Manthiram, A. A Reflection on Lithium-Ion Battery Cathode Chemistry. *Nature Communications*. Nature Research December 1, 2020, pp 1–9.

(4) Younesi, R.; Veith, G. M.; Johansson, P.; Edström, K.; Vegge, T. Lithium Salts for Advanced Lithium Batteries: Li-Metal, Li-O2, and Li-S. *Energy and Environmental*

Science. Royal Society of Chemistry July 1, 2015, pp 1905–1922.
(5) Eshetu, G. G.; Bertrand, J. P.; Lecocq, A.; Grugeon, S.; Laruelle, S.; Armand, M.; Marlair, G. Fire Behavior of Carbonates-Based Electrolytes Used in Li-Ion Rechargeable Batteries with a Focus on the Role of the LiPF6 and LiFSI Salts. *J. Power Sources* **2014**, *269*, 804–811.
(6) Zhao, W.; Yi, J.; He, P.; Zhou, H. Solid-State Electrolytes for Lithium-Ion Batteries: Fundamentals, Challenges and Perspectives. *Electrochem. Energy Rev.* **2019**, *2* (4), 574–605.
(7) Zhou, D.; Shanmukaraj, D.; Tkacheva, A.; Armand, M.; Wang, G. Polymer Electrolytes for Lithium-Based Batteries: Advances and Prospects. *Chem*. Elsevier Inc September 12, 2019, pp 2326–2352.
(8) Jones, S. D.; Schauser, N. S.; Fredrickson, G. H.; Segalman, R. A. The Role of Polymer-Ion Interaction Strength on the Viscoelasticity and Conductivity of Solvent-Free Polymer Electrolytes. *Macromolecules* **2020**, *53* (23), 10574–10581.
(9) Schauser, N. S.; Sanoja, G. E.; Bartels, J. M.; Jain, S. K.; Hu, J. G.; Han, S.; Walker, L. M.; Helgeson, M. E.; Seshadri, R.; Segalman, R. A. Decoupling Bulk Mechanics and Mono- and Multivalent Ion Transport in Polymers Based on Metal–Ligand Coordination. *Chem. Mater.* **2018**, *30* (16), 5759–5769.
(10) Schauser, N. S.; Nikolaev, A.; Richardson, P. M.; Xie, S.; Johnson, K.; Susca, E. M.; Wang, H.; Seshadri, R.; Clément, R. J.; Read De Alaniz, J.; et al. Glass Transition Temperature and Ion Binding Determine Conductivity and Lithium-Ion Transport in Polymer Electrolytes. *ACS Macro Lett.* **2021**, *10* (1), 104–109.
(11) Ihmels, E. C.; Gmehling, J. Extension and Revision of the Group Contribution Method GCVOL for the Prediction of Pure Compound Liquid Densities. *Ind. Eng. Chem. Res.* **2003**, *42* (2), 408–412.
(12) Krevelen, D. W. Van; Hoftyzer, P. J. Prediction of Polymer Densities. *J. Appl. Polym. Sci.* **1969**, *13* (5), 871–881.
(13) Hawkes, M. J. B.; Billig, E.; Gray, H. B. Characterization and Electronic Structures of Metal Complexes Containing Benzene-1,2-Dithiolate and Related Ligands. *J. Am. Chem. Soc.* **1966**, *88* (21), 4870–4875.
(14) Eisenberg, R.; Gray, H. B. Noninnocence in Metal Complexes: A Dithiolene Dawn. *Inorg. Chem.* **2011**, *50* (20), 9741–9751.
(15) Jørgensen, C. K. Differences between the Four Halide Ligands, and Discussion Remarks on Trigonal-Bipyramidal Complexes, on Oxidation States, and on Diagonal Elements of One-Electron Energy. *Coord. Chem. Rev.* **1966**, *1* (1–2), 164–178.
(16) Luca, O. R.; Crabtree, R. H. Redox-Active Ligands in Catalysis. *Chem. Soc. Rev.* **2013**, *42* (4), 1440–1459.
(17) Wu, J.; Zuo, X.; Chen, Q.; Deng, X.; Liang, H.; Zhu, T.; Liu, J.; Li, W.; Nan, J. Functional Composite Polymer Electrolytes with Imidazole Modified SiO2 Nanoparticles for High-Voltage Cathode Lithium Ion Batteries. *Electrochim. Acta* **2019**, *320*, 134567.
(18) Zhang, Q.; Liu, K.; Liu, K.; Zhou, L.; Ma, C.; Du, Y. Imidazole Containing Solid Polymer Electrolyte for Lithium Ion Conduction and the Effects of Two Lithium Salts. *Electrochim. Acta* **2020**, *351*, 136342.
(19) Hansch, C.; Leo, A.; Taft, R. W. A Survey of Hammett Substituent Constants and Resonance and Field Parameters. *Chem. Rev.* **2002**, *91* (2), 165–195.
(20) Charton, M. The Upsilon Steric Parameter — Definition and Determination. *Steric Eff. Drug Des.* **1983**, 57–91.
(21) Hansch, C.; Leo, A.; Taft, R. W. A Survey of Hammett Substituent Constants and Resonance and Field Parameters. *Chem. Rev.* **1991**, *91* (2), 165–195.
(22) Gardner Swain, C.; Lupton, E. C. Field and Resonance Components of Substituent Effects. *J. Am. Chem. Soc.* **1968**, *90* (16), 4328–4337.
(23) Zhang, Y.; Maginn, E. J. Direct Correlation between Ionic Liquid Transport Properties and Ion Pair Lifetimes: A Molecular Dynamics Study. *J. Phys. Chem. Lett.* **2015**, *6* (4), 700–705.
(24) Schauser, N. S.; Grzetic, D. J.; Tabassum, T.; Kliegle, G. A.; Le, M. L.; Susca, E. M.;

Antoine, S.; Keller, T. J.; Delaney, K. T.; Han, S.; et al. The Role of Backbone Polarity on Aggregation and Conduction of Ions in Polymer Electrolytes. *J. Am. Chem. Soc.* **2020**, *142* (15), 7055–7065.
(25) Sharon, D.; Bennington, P.; Webb, M. A.; Deng, C.; De Pablo, J. J.; Patel, S. N.; Nealey, P. F. Molecular Level Differences in Ionic Solvation and Transport Behavior in Ethylene Oxide-Based Homopolymer and Block Copolymer Electrolytes. *J. Am. Chem. Soc.* **2021**.
(26) Zhang, Z.; Wheatle, B. K.; Krajniak, J.; Keith, J. R.; Ganesan, V. Ion Mobilities, Transference Numbers, and Inverse Haven Ratios of Polymeric Ionic Liquids. *ACS Macro Lett.* **2020**, *9*, 84–89.
(27) Nordness, O.; Brennecke, J. F. Ion Dissociation in Ionic Liquids and Ionic Liquid Solutions. *Chem. Rev.* **2020**, *120*, 12873–12902.